SARS-CoV-2 Causes a Specific Dysfunction of the Kidney Proximal Tubule

Werion, Alexis ; Belkhir, Leila ; Perrot, Marie ; et al ; Chen, Zhiyong ; Devuyst, Olivier

Abstract: Coronavirus disease 2019 (COVID-19) is commonly associated with kidney damage, and the angiotensin converting enzyme 2 (ACE2) receptor for SARS-CoV-2 is highly expressed in the proximal tubule cells. Whether patients with COVID-19 present specific manifestations of proximal tubule dysfunction remains unknown. To test this, we examined a cohort of 49 patients requiring hospitalization in a large academic hospital in Brussels, Belgium. There was evidence of proximal tubule dysfunction in a subset of patients with COVID-19, as attested by low-molecular-weight proteinuria (70-80%), neutral aminoaciduria (46%), and defective handling of uric acid (46%) or phosphate (19%). None of the patients had normoglycemic glucosuria. Proximal tubule dysfunction was independent of pre-existing comorbidities, glomerular proteinuria, nephrotoxic medications or viral load. At the structural level, kidneys from patients with COVID-19 showed prominent tubular injury, including in the initial part of the proximal tubule, with brush border loss, acute tubular necrosis, intraluminal debris, and a marked decrease in the expression of megalin in the brush border. Transmission electron microscopy identified particles resembling coronaviruses in vacuoles or cisternae of the endoplasmic reticulum in proximal tubule cells. Among features of proximal tubule dysfunction, hypouricemia with inappropriate uricosuria was independently associated with disease severity and with a significant increase in the risk of respiratory failure requiring invasive mechanical ventilation using Cox (adjusted hazard ratio 6.2, 95% CI 1.9-20.1) or competing risks (adjusted sub-distribution hazard ratio 12.1, 95% CI 2.7-55.4) survival models. Thus, our data establish that SARS-CoV-2 causes specific manifestations of proximal tubule dysfunction and provide novel insights into COVID-19 severity and outcome.

DOI: https://doi.org/10.1016/j.kint.2020.07.019

Since January 2020 Elsevier has created a COVID-19 resource centre with free information in English and Mandarin on the novel coronavirus COVID-19. The COVID-19 resource centre is hosted on Elsevier Connect, the company's public news and information website.

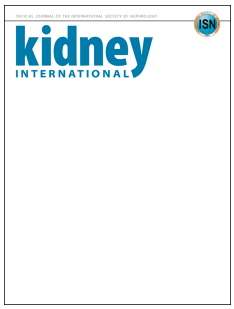

SARS-CoV-2 Causes a Specific Dysfunction of the Kidney Proximal Tubule

Alexis Werion, Leila Belkhir, Marie Perrot, Gregory Schmit, Selda Aydin, Zhiyong Chen, Andrea Penaloza, Julien De Greef, Halil Yildiz, Lucie Pothen, Jean Cyr Yombi, Joseph Dewulf, Anais Scohy, Ludovic Gérard, Xavier Wittebole, Pierre-François Laterre, Sara E. Miller, Olivier Devuyst, Michel Jadoul, Johann Morelle, on behalf of the CUSL COVID-19 Research Group

PII: S0085-2538(20)30912-1

DOI: https://doi.org/10.1016/j.kint.2020.07.019

Reference: KINT 2235

To appear in: *Kidney International*

Received Date: 8 May 2020

Revised Date: 14 July 2020

Accepted Date: 16 July 2020

Please cite this article as: Werion A, Belkhir L, Perrot M, Schmit G, Aydin S, Chen Z, Penaloza A, De Greef J, Yildiz H, Pothen L, Yombi JC, Dewulf J, Scohy A, Gérard L, Wittebole X, Laterre PF, Miller SE, Devuyst O, Jadoul M, Morelle J, on behalf of the CUSL COVID-19 Research Group, SARS-CoV-2 Causes a Specific Dysfunction of the Kidney Proximal Tubule, *Kidney International* (2020), doi: https://doi.org/10.1016/j.kint.2020.07.019.

SARS-CoV-2 Causes a Specific Dysfunction of the Kidney Proximal Tubule

49 patients with COVID-19 requiring hospitalization (Saint-Luc Academic Hospital, Brussels, Belgium)

Proximal tubule (PT) dysfunction

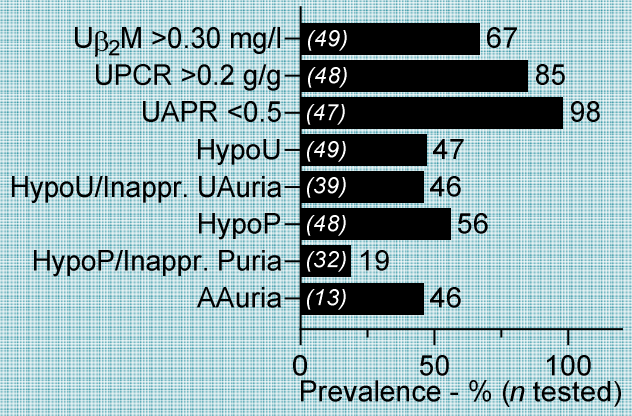

Independent from comorbidities, glomerular proteinuria, nephrotoxic medications or viral load

Association with severity and outcome of COVID-19

Features of PT dysfunction (i.e. defective tubular handling of uric acid)

- Nadir lymphocyte count, peak hsCRP/LDH/D-dimers
- Invasive mechanical ventilation (Cox and competing risks models)

Structural/ultrastructural level

PT injury, decreased expression of megalin in brush border, particles resembling SARS-CoV-2 in PT cells

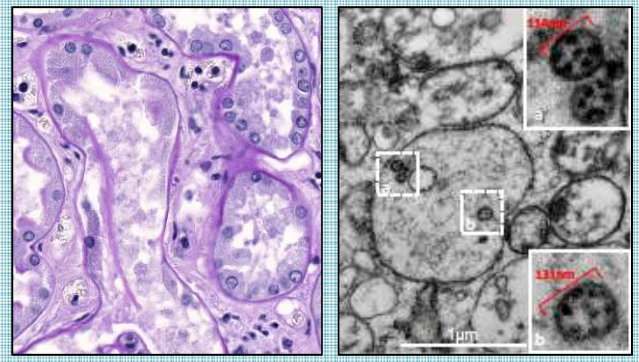

CONCLUSION:

SARS-CoV-2 causes specific manifestations of PT dysfunction including low molecular weight proteinuria, neutral aminoaciduria, and defective handling of uric acid and phosphate

kidney INTERNATIONAL
OFFICIAL JOURNAL OF THE INTERNATIONAL SOCIETY OF NEPHROLOGY

Werion, Belkhir et al, 2020

KI-05-20-0820.R3

[QUERY TO AUTHOR: title and abstract rewritten by Editorial Office – not subject to change]

SARS-CoV-2 Causes a Specific Dysfunction of the Kidney Proximal Tubule

Alexis Werion[1]*, Leila Belkhir[2,7]*, Marie Perrot[1], Gregory Schmit[3,6], Selda Aydin[3,7], Zhiyong Chen[8], Andrea Penaloza[4], Julien De Greef[2,7], Halil Yildiz[2,7], Lucie Pothen[2,7], Jean Cyr Yombi[2,7], Joseph Dewulf[3], Anais Scohy[3], Ludovic Gérard[5,7], Xavier Wittebole[5,7], Pierre-François Laterre[5,7], Sara E. Miller[9], Olivier Devuyst[1,7,8]*¶, Michel Jadoul[1,7]*¶, and Johann Morelle[1,7]*¶, on behalf of the CUSL COVID-19 Research Group

[1]Division of Nephrology, [2]Division of Internal Medicine and Infectious Diseases, [3]Department of Laboratory Medicine, Microbiology and Pathology, [4]Department of Emergency Medicine; [5]Department of Intensive Care Medicine; and [6]Centre of Forensic Medicine, Cliniques universitaires Saint-Luc, Brussels, Belgium; [7]Institut de Recherche Expérimentale et Clinique, UCLouvain, Brussels, Belgium; [8]Department of Physiology, Mechanisms of Inherited Kidney Disorders Group, University of Zurich, Zurich, Switzerland; [9]Department of Pathology, Duke University Medical Center, Durham, NC, USA.

* Equal contribution; ¶ Equal contribution, co-directed the study.

Correspondence: Johann Morelle, Division of Nephrology, Cliniques universitaires Saint-Luc, Avenue Hippocrate 10, B-1200 Brussels, Belgium, T +32 2 7641855, F +32 2 7642836, Email: johann.morelle@uclouvain.be.

Running title: Proximal tubule dysfunction in COVID-19

Keywords: COVID-19, kidney, renal Fanconi syndrome; severe acute respiratory syndrome

ABSTRACT

Coronavirus disease 2019 (COVID-19) is commonly associated with kidney damage, and the angiotensin converting enzyme 2 (ACE2) receptor for SARS-CoV-2 is highly expressed in the proximal tubule cells. Whether patients with COVID-19 present specific manifestations of proximal tubule dysfunction remains unknown. To test this, we examined a cohort of 49 patients requiring hospitalization in a large academic hospital in Brussels, Belgium. There was evidence of proximal tubule dysfunction in a subset of patients with COVID-19, as attested by low-molecular-weight proteinuria (70-80%), neutral aminoaciduria (46%), and defective handling of uric acid (46%) or phosphate (19%). None of the patients had normoglycemic glucosuria. Proximal tubule dysfunction was independent of pre-existing comorbidities, glomerular proteinuria, nephrotoxic medications or viral load. At the structural level, kidneys from patients with COVID-19 showed prominent tubular injury, including in the initial part of the proximal tubule, with brush border loss, acute tubular necrosis, intraluminal debris, and a marked decrease in the expression of megalin in the brush border. Transmission electron microscopy identified particles resembling coronaviruses in vacuoles or cisternae of the endoplasmic reticulum in proximal tubule cells. Among features of proximal tubule dysfunction, hypouricemia with inappropriate uricosuria was independently associated with disease severity and with a significant increase in the risk of respiratory failure requiring invasive mechanical ventilation using Cox (adjusted hazard ratio 6.2, 95% CI 1.9-20.1) or competing risks (adjusted sub-distribution hazard ratio 12.1, 95% CI 2.7-55.4) survival models. Thus, our data establish that SARS-CoV-2 causes specific manifestations of proximal tubule dysfunction and provide novel insights into COVID-19 severity and outcome.

INTRODUCTION

The recent pandemic of coronavirus disease 2019 (COVID-19) caused by the severe acute respiratory syndrome coronavirus-2 (SARS-CoV-2) has major public health and economic impact [1]. The clinical spectrum of COVID-19 is broad, ranging from asymptomatic carrier state to severe, bilateral and diffuse pneumonia, potentially leading to acute respiratory distress syndrome (ARDS), respiratory failure, and/or multiple organ dysfunction[2,3]. Identifying early manifestations of COVID-19 and patients at risk for disease progression and respiratory failure is of crucial importance to alleviate the major stress on healthcare systems.

The angiotensin converting enzyme 2 (ACE2), the receptor mediating the entry of SARS-CoV-2 in human cells, is expressed in the lung, heart, intestine and kidney, providing a rationale for the systemic manifestations of the disease[4-7]. Increasing evidence suggests that COVID-19 may cause kidney damage, as indicated by the occurrence of proteinuria, hematuria and elevated serum creatinine on admission; the high incidence of acute kidney injury (AKI); and a spectrum of pathologic abnormalities including acute tubular necrosis, endothelial damage and capillary occlusions, deposition of complement complex on tubules, and glomerular lesions identified in autopsy reports[8-13]. Kidney damage may result from hemodynamic factors, dysfunctional immune responses[14], or direct viral infection of kidney cells, the latter being compatible with the detection of SARS-CoV-2 mRNA and protein in glomerular and tubular cells[15] and of purported viral particles in podocytes and proximal tubule (PT) cells[8,16-17]. However, the identification of viral particles by electron microscropy is challenging, as they may easily be mistaken for normal cell organelles such as the endoplasmic reticulum (ER), clathrin-coated vesicles, or multivesicular bodies[18-20].

Overall, several arguments suggest the PT may be a specific target for SARS-CoV-2 infection. Here, we analyzed the characteristics, extent and structural correlates of PT dysfunction in a cohort of patients admitted with SARS-CoV-2 infection in a large academic

hospital in Brussels, Belgium. We further investigated the association of various markers of PT dysfunction with COVID-19 severity and outcome.

RESULTS

Study population

The detection of proteinuria of unknown mechanism by routine analysis among ~80 % of patients in the early phase of the pandemic prompted us to perform specific urinalyses in 49 patients with documented SARS-Cov-2 infection hospitalized at the Cliniques universitaires Saint-Luc in Brussels, Belgium, between March 31, 2020 and April 18, 2020 (Suppl. Fig. 1). Patients on kidney replacement therapy at the time of admission were excluded.

Baseline characteristics of the 49 patients with specific urinalysis are presented in Table 1. Median age (interquartile range, IQR) at admission was 64 years (54-74) and 69% were males; 86% were of Caucasian and 12% of Sub-Saharan African origin. Eighteen percent, 47%, 20%, and 14% had a history of cardiovascular disease, hypertension, diabetes and chronic kidney disease, respectively. Chronic kidney disease was ascribed to hypertension (n=2, 29%), chronic interstitial nephritis (n = 2, 29%), nephron mass reduction (n=1, 14 %), or unknown origin (n=2, 29%). Forty percent were treated with a renin angiotensin system inhibitor. Eight percent were on chronic immunosuppressive treatment and another 8% on anti-cancer therapy. A detailed list of these medications is provided in Table 1.

Patients were admitted a median (IQR) of 7 days (3-9) after the onset of symptoms, mainly with fever (80%), dyspnea (71%) and cough (59%) (Table 1). Almost all patients (47/49, 96%) were admitted via the emergency room. At admission, median oxygen saturation while breathing ambient air was 92% (87-96); highly sensitive C-reactive protein, 105 mg/l (54-146); glomerular filtration rate estimated by the CKD-EPI equation (eGFR), 72 ml/min/1.73 m² (54-92); and lymphocyte count, 650 per µl (500-1060). The extent of pulmonary lesions at admission, quantified using computed tomography[21], was as follows: <10%, 9% of the patients; 10-25%, 40%; 25-50%, 31%; and >50%, 20%. Most patients were

hospitalized in dedicated COVID-19 units (n=40, 82%), while a minority (n=9, 18%) was directed to a dedicated intensive care unit. During hospitalization, 48 patients (98%) received hydroxychloroquine and 16 (33%) immunomodulatory drugs for COVID-19. No patient was treated with anti-viral drugs (Table 1). The 166 patients with routine urinalysis who presented between February 23, 2020 and April 18, 2020 had similar baseline characteristics (Suppl. Table 1).

Proximal tubule dysfunction in COVID-19

Specific urinalyses, performed a median (IQR) of 9 days (3-16) after admission, assessed the occurrence and pattern of PT dysfunction in patients with COVID-19 (Fig. 1; Table 2; Suppl. Fig. 2). Among the 49 COVID-19 patients, 69% (33/49) had elevated urinary levels of β2-microglobulin; 85% (41/48 tested), a urinary protein to creatinine ratio (UPCR) >0.2 g/g; and 98% (46/47), a urinary albumin to protein ratio (UAPR) <0.5 (Fig. 1A and 1B; Table 2). Electrophoresis of urine samples from COVID-19 patients evidenced multiple protein bands below 70 kDa (low-molecular-weight [LMW] proteinuria), which included the vitamin D-binding protein (DBP) and Clara cell secretory protein (CC16). These bands, which were not detected in healthy controls, are similar to those detected in the urine of patients with congenital PT dysfunction due to Dent disease, toxic acute tubular necrosis secondary to tenofovir, or heavy proteinuria caused by nephrotic syndrome (Fig. 1D; Suppl. Fig. 3; Suppl. Table 2). The prevalence of proteinuria was similar between patients without or with diabetes (UPCR >0.2 g/g: 84% vs 90%, P=0.64) and between patients without or with history of CKD (UPCR >0.2 g/g: 86% vs 83%, P=0.88). Heavy proteinuria (UPCR >2.5 g/g) was identified in 2 patients, and one had selective albuminuria (UAPR >0.5). The first had heavy proteinuria months before COVID-19, suggesting unrelated kidney disease, while no past urinalysis was available in the other.

Forty-seven percent (23/49) and 56% (27/48) of the patients had hypouricemia and/or hypophosphatemia, respectively (Fig. 1A; Table 2). Inappropriate uricosuria (fractional excretion of uric acid [FE_{UA}] >10%) was observed in 90% (18/20) of the patients with hypouricemia, and defective tubular handling of uric acid (hypouricemia with inappropriate uricosuria) was found in 46% (18/39 tested) of the cohort (Fig. 1A; Fig. 1C; Table 2). Hypophosphatemia with inappropriate phosphaturia (FE_P >20%) was observed in 19% (6/32).

Aminoaciduria was detected in 6 out of 13 (46%) tested COVID-19 patients (Fig. 1A; Table 2), and was restricted to neutral amino acids (Fig. 1E; Suppl. Table 3), a pattern similar to that found in Hartnup disease, caused by recessive mutations in *SCL6A19*, which encodes the amino acid transporter B^0AT1 (SLC6A19) [22,23]. Of interest, B^0AT1 interacts with ACE2 [6,23], both highly expressed in PT cells of the normal human kidney (Suppl. Fig. 4A,C,D). Transcriptomic analysis of specific segments of the mouse nephron confirmed the enrichment of genes encoding for the SARS-Cov-2 receptor ACE2, its homologue TMEM27 (collectrin), uric acid transporter URAT1 (SLC22A12), sodium-dependent phosphate cotransporter NaPi-IIa (SLC34A1), and B0AT1 in PT segments (Suppl. Fig. 4B).

Three out of the 43 patients tested had positive dipstick glucosuria upon admission. Two of them had a history of type 2 diabetes, concomitant hyperglycemia and significant glucosuria (blood glucose 215 mg/dl and 331 mg/dl; and dipstick glucosuria 2+ and 4+, respectively), while the remaining individual had prediabetes (HbA1c 6.0%), slightly elevated blood glucose (127 mg/dl) and mild glucosuria (1+). In contrast with other signs of PT dysfunction, none of the patients in the cohort showed normoglycemic glucosuria (Table 2).

Altogether, these observations showed that a specific dysfunction of the PT develops in a subset of patients with severe forms of COVID-19, occurs early during the course of the disease and is characterized by LMW proteinuria, defective handling of uric acid and phosphate, and neutral aminoaciduria.

Proximal tubule dysfunction, clinical presentation, disease severity and outcomes

To assess the potential clinical relevance of PT dysfunction in patients hospitalized with COVID-19, we compared the clinical presentation, disease severity and outcomes of patients with versus without elevated urinary β2-microglobulin, defective handling of uric acid and phosphate, or aminoaciduria (Suppl. Tables 4-7).

Biological signs of PT dysfunction were not associated with demographics, disease presentation or severity, or viral load, estimated from real time polymerase chain reaction and cycle threshold (Ct) values at admission. They were also independent from comorbidities, medications interfering with uric acid production or with potential PT toxicity, including anti-viral or immunomodulatory drugs (Table 1; Suppl. Table 1).

Patients with defective handling of uric acid (i.e. hypouricemia with inappropriate uricosuria), who also had higher prevalence of LMW proteinuria, aminoaciduria and defective handling of phosphate (Suppl. Table 5), showed higher disease severity as compared with others. This was evidenced by a lower nadir of lymphocyte count (median [IQR]: 250 per µl [100-360] vs 500 per µl [280-910, P=0.006), and higher peak values of hsCRP (324 mg/dl [243-349] vs 126 mg/dl [51-245], P=0.002), LDH (584 IU/l [524-726] vs 394 IU/l [317-466], P<0.001), and D-dimers (4461 ng/ml [2098-13348) vs 1234 ng/ml [753-2827], P=0.001), in these patients compared to those without inappropriate uricosuria (Suppl. Table 5).

During a median follow-up (IQR) of 44 days (31-56), 19/49 patients (39%) in the cohort required invasive mechanical ventilation, 14 (29%) died, 11 (22%) developed AKI; and 2 (4%) required kidney replacement therapy (Suppl. Fig. 1; Suppl. Table 1). Hypouricemia with inappropriate uricosuria was associated with a higher occurrence of invasive mechanical ventilation (83% vs 14%, P<0.001) and death (50% vs 14%, P=0.02) and with longer hospital stay (27 days [17-46] vs 12 [6-17], P<0.001), compared to patients with

normal tubular handling of uric acid (Suppl. Table 5). Time-to-event analyses using Cox regressions showed an independent association between defective tubular handling of uric acid and higher risk of invasive mechanical ventilation or death (adjusted hazard ratio [HR] 6.2, 95% confidence interval [CI] 1.9-20.1, P=0.002). An alternative approach considering death and discharge from hospital as competing events confirmed the independent association between tubular loss of uric acid and the need for invasive mechanical ventilation (adjusted subdistribution HR 12.1, 95% CI 2.7-55.4, P=0.001) (Suppl. Table 8).

Proximal tubule damage in kidneys of COVID-19 patients

To characterize structural alterations associated with PT dysfunction, we analyzed 6 kidney autopsy samples from patients who died of COVID-19, for whom tissue samples were well-preserved with absence of autolysis at the optical level. The patients' age ranged between 57 and 82 years; 4 were males; all had abnormal proteinuria and 2 developed AKI requiring kidney replacement therapy (Suppl. Table 9). None of the patients received anti-viral medications.

Post-mortem examination of the COVID-19 kidneys showed prominent and diffuse PT damage in all patients, with dilation of the tubular lumen containing cellular debris, denuded basement membranes and major alterations of the brush border (Fig. 2A; Suppl. Fig. 5; Suppl. Table 10). In addition to tubular lesions, erythrocyte aggregates in peritubular and/or glomerular capillaries were found in 5 out of the 6 patients. One patient with moderate proteinuria (UPCR 0.7 g/g) showed a single lesion of focal and segmental glomerulosclerosis (tip lesion variant). Focal infiltration of the interstitium by mononuclear cells was observed in 2 out of the 6 patients.

Confocal microscopy examination revealed that the expression of the multi-ligand receptor megalin (LRP2), which mediates the reabsorption of LMW proteins at the apical

membrane of PT cells, was severely decreased (~50%) in the PT cells of patients with COVID-19, compared to the normal kidney (Fig. 2B). The decreased expression of megalin contrasted with the stable (trend to increased) expression of ACE2 in PT cells of COVID-19 kidneys (Suppl. Fig. 4A).

Transmission electron microscopy identified particles resembling coronaviruses in vacuoles or cisternae of the ER in PT cells (Fig. 3). They measured between 90 and 140 nm and contained small dense irregular dots of 10-20 nm. Some particles were budding into the ER lumen, and a few had faint wisps of projections on their surfaces that contacted the luminal contents, not the cytoplasm. A trilaminar envelope was identified around some particles. Some of the particles contained few (1 to 3) crisp, dense circles of 10-15 nm. Ultrastructurally, the tissue was degraded as expected from the pathology observations.

DISCUSSION

In this cohort of patients hospitalized for SARS-CoV-2 infection, we provide direct evidence that PT dysfunction develops in a subset of patients with COVID-19 and is characterized by LMW proteinuria, hypophosphatemia and hypouricemia due to inappropriate urinary loss of phosphate and uric acid, and neutral aminoaciduria. The PT dysfunction is independent from pre-existing kidney disease, glomerular proteinuria, viral load, or toxic medications. Defective tubular handling of uric acid is independently associated with disease severity and with a higher incidence of respiratory failure requiring mechanical ventilation. Analyses of autopsy kidney samples revealed tubular damage, defective expression of megalin, and presence of particles resembling coronaviruses in vacuoles or ER cisternae in PT cells.

Our data document that COVID-19 causes a specific dysfunction of the PT. The PT cells reabsorb a large amount of ions, solutes and LMW proteins, using specialized transport systems that operate in their apical membrane[24]. These transport systems include multi-ligand receptors such megalin, the urate transporter URAT1 (SLC22A12), the sodium-dependent phosphate cotransporters NaPi-IIa (SLC34A1) and NaPi-IIc (SLC34A3), and amino acid transporters such the sodium-dependent neutral amino acid transporter B^0AT1 (SLC6A19)[23,25,26]. Impairment of PT transport processes leads to the urinary loss of LMW proteins and solutes (e.g., amino acids, uric acid, phosphate), a clinical entity called renal Fanconi syndrome. The PT dysfunction can result from inherited disorders (e.g., Dent disease, Lowe syndrome, cystinosis), or be acquired (monoclonal light chains, toxins, drugs, autoimmune disorders)[27]. The PT dysfunction detected in patients with COVID-19 variably includes LMW proteinuria, aminoaciduria, and inappropriate urinary loss of uric acid and phosphate but not of glucose. This corresponds to a partial renal Fanconi syndrome, as observed in other PT disorders[24,27-29]. The molecular mechanisms accounting for such specific defects remain mostly unknown.

Post-mortem examination of kidneys from patients with COVID-19 showed prominent lesions of PT injury, including loss of brush border, cell necrosis, and intra-luminal debris, in line with previous reports [16]. These lesions are associated with a ~50% reduction in the apical staining for megalin in PT cells. Studies in model organisms and congenital disorders including Donnai-Barrow syndrome, caused by mutations in the *LRP2* gene coding for megalin, or Dent disease, caused by mutations in the *CLCN5* gene coding for the endosomal chloride-proton exchanger ClC-5, have highlighted the critical role of megalin in the reabsorption of LMW ligands by PT cells[24,25,30]. Of note, alteration of megalin expression in patients with COVID-19 was also observed in patients with tenofovir-induced PT dysfunction[31], confirming the defect is not restricted to COVID-19. Conversely, the expression of megalin is preserved in patients presenting acute tubular injury without overt PT dysfunction, related e.g. to sepsis, aminoglycosides, or hepatorenal syndrome[31].

The fact that PT cells highly express ACE2 suggests that they could be targeted by SARS-CoV-2 at an early stage of disease. The binding affinity of SARS-CoV-2 spike glycoprotein to ACE2 is a major determinant of disease severity[32]. Besides its role in the renin angiotensin system, ACE2 facilitates the trafficking of B^0AT1 to the apical membrane[23]. Recent studies reported the cryo-electron microscopy structure of the full-length human ACE2, forming heterodimers with B^0AT1[6]. The aminoaciduria observed in patients with COVID-19 is essentially composed of neutral amino acids, similar to that encountered in patients with Hartnup disorder, caused by recessive, loss-of-function mutations in B^0AT1. As B^0AT1 requires ACE2 (or the related protein collectrin) for its apical targeting in epithelial cells, one could speculate that SARS-CoV-2 binding and entry may lead to a partial dysfunction of the amino acid transporter, causing mild neutral aminoaciduria. The fact that B^0AT1 is not directly affected by SARS-CoV-2 explains the moderate loss in patients with COVID-19 compared to Hartnup disease. The downregulation of specific tubule transporters,

including URAT1, caused by viral mimetics in experimental models also supports a causative link between infection and PT dysfunction[33].

SARS-CoV-2 may damage the kidney by various mechanisms, including direct viral infection. The presence of SARS-CoV-2 RNA and shedding of viable SARS-CoV-2 in the urine have been reported[34,35]. SARS-CoV-2 is able to infect human kidney organoids expressing ACE2 and PT cell markers, with inhibition by soluble recombinant human ACE2[36]. Particles resembling coronavirus have been described in kidney samples from autopsied COVID-19 patients[16,17,37]. Several articles have refuted this data, and these structures have been identified as clathrin-coated vesicles or multivesicular bodies[19,20]. The particles shown here are uniform in size and appearance and are of the right size (90-140 nm) and similar morphology to coronaviruses. They are located inside vacuoles or ER lumens and show faint hints of projections in contact with the vacuolar contents - not the cell cytoplasm[19]. Also, the particles contain dense dots (10-15 nm), forming either crisp circles or larger, smudgy dots, that may correspond to sections across the tube- or helix-forming of the virus nucleocapsid[38,39]. Of note, most dots inside these particles appear larger than nucleocapsids observed in properly fixed tissue cultures[38,39]. These dots are approximately the size of ribosomes (~20 nm); however, only arenaviruses appear to contain ribosomes and, to our knowledge, no normal cell structures appear like this. Alternatively, the larger-than-expected (for a nucleocapsid) and irregularly shaped dense dots could be related to poor fixation and delay in processing[38,39].

In cells containing these virus-like structures, the particles are more uniform in size than any normal cell architecture, such as secretory granules, and they do not have the solid dark center of dense granules. With the limitations stated above, we believe that identified particles resemble viruses in most respects and are possible candidates for coronaviruses in

PT cells. Because many intracellular particles can masquerade as viruses[40-41], further analyses including immunoelectron microscopy are necessary to prove their identification as viruses.

Despite the small cohort size, our observations suggest that the presence of hypouricemia due to impaired tubular handling of uric acid, a marker of PT dysfunction, associates with disease severity and outcomes, in particular the need for invasive mechanical ventilation. Interestingly, hypouricemia, was common and associated with poor outcome in patients with SARS[42]. Potential mechanisms linking PT dysfunction and respiratory failure may include the loss of important solutes, including uric acid, which may affect defense against oxidative stress and respiratory function[43]. Genetic factors regulating SARS Cov-2 entry into host cells may also contribute to multi-organ severity in COVID-19. Of note, we did not observe any association between PT dysfunction and viral load, nephrotoxic medications or comorbidities. Finally, although almost all patients were given the drug, hydroxychloroquine does not cause PT toxicity. If these findings are validated, markers of PT dysfunction might be useful for the initial work-up of COVID-19 patients and for identifying patients at risk for progression to severe disease.

The strengths of this study include the availability of a large cohort of well-characterized patients admitted via the emergency room; standardized protocols of treatment; detailed characterization of PT dysfunction; outcome analysis; correlations with viral load; and analyses on kidney samples from patients with COVID-19. Our work also has limitations, including the lack of standardized characterization of PT markers in all patients at admission, with limited number of measurement for some markers; and the single centre design of the study, requiring confirmation. Although sensitivity analyses suggest that patients included in this study are representative of the whole cohort, the true prevalence of PT dysfunction among patients with COVID-19 needs to be substantiated in prospective studies.

In summary, SARS-CoV-2 infection causes an early and specific dysfunction of the kidney PT characterized by LMW proteinuria, defective tubular handling of uric acid and phosphate and neutral aminoaciduria. These transport defects are associated with structural and molecular alterations of PT cells, and detection of particles resembling coronaviruses. The presence of hypouricemia and inappropriate uricosuria associates with disease severity and outcome. These data provide novel insights into the pathophysiology of COVID-19 and open perspectives for biomarkers of disease severity.

METHODS

Study design and patients

The very first patient with COVID-19 was admitted to our hospital on February 23, 2020. All consecutive adult patients, admitted between February 23, 2020 and April 18, 2020, at Cliniques universitaires Saint- Luc (CUSL), Brussels, Belgium with a SARS-CoV2-associated pneumonia were enrolled in a prospective registry. The diagnosis was based on a positive SARS-CoV2 Real-Time RT-PCR on nasopharyngeal swab or broncho-alveolar lavage combined with suggestive abnormalities on chest X-ray or computed tomography.

As the number of cases exponentially increased in March 2020, 7 additional units of 20 beds were dedicated to COVID-19 to accommodate the flux of patients. They were all staffed with two fellows and two senior physicians from internal medicine or a related discipline (pulmonology, nephrology, cardiology, hepatogastroenterology, hematology, oncology, geriatrics). The infectious disease specialists supervised the general management and provided continuous expert advice.

As the pandemic progressed, we realized that routine urinalysis showed proteinuria of unknown mechanism in around 80% of patients with COVID-19 already upon admission. This prompted us to subsequently order specific urinalyses in 49 patients with documented SARS-Cov-2 infection hospitalized at the Cliniques universitaires Saint-Luc between March 31, 2020 and April 18, 2020 (Suppl. Fig. 1). Patients on kidney replacement therapy at the time of admission (hemodialysis, peritoneal dialysis or kidney transplantation) were not included in this study. During the study period, 68 consecutive patients with SARS-Cov-2 infection were admitted to our institution.

The standard treatment for patients hospitalized for COVID-19 at that time included hydroxychloroquine 400 mg b.i.d. on the first hospital day then 200 mg b.i.d. for 4 additional

days in patients without contraindication, as recommended by the Belgian COVID-19 interim guidelines. Patients were followed until death or end of study follow-up, on May 22, 2020.

The study was conducted in accordance with the World Medical Association's Declaration of Helsinki, the Belgian law related to experiments in humans dated May 7, 2004, the General Data Protection Regulation 2016/679 and the Belgian law of July 30, 2018 regarding the protection of personal data. The Ethical Review Board of Cliniques universitaires Saint-Luc/UCLouvain approved the study and waived the requirement to obtain informed consent based on the observational design.

Data collection and definitions

The following data were extracted from electronic medical records: demographics, symptoms at admission, unit where the patient was hospitalized first (intensive care unit versus conventional unit), vital signs, biological and imaging data, and outcome. We recorded routine biological data obtained at admission, as well as the nadir lymphocyte count, and the peak values for highly sensitive C-reactive protein, lactate dehydrogenase and D-dimers during hospitalization. Dipstick urinalysis (glucose, proteins) was performed at the time of admission. The frequent observation of abnormal positive dipstick proteinuria in the first patients prompted subsequent measurement of urinary levels of electrolytes, proteins, albumin, creatinine, $ß_2$-microglobulin, and eventually amino acids for consecutive patients during hospitalization. Data were checked by three physicians (AW, MP, JM) and reviewed in collaboration with a fourth one (MJ).

Lab measurements were performed, unless otherwise mentioned, on an automated Roche Cobas 8000 analyzer, equipped with modules ISE, c702, c502 and e602 (Roche diagnostics, Rotkreuz, ZG, Switzerland), or a UC3500 automated urine analyzer (Sysmex). Urinary levels of β2-microglobulin were expressed as concentration, using an upper limit of

normal of 0.3 mg/l (mean ± 2 SD in healthy subjects)[44]. In our cohort, the urinary concentration of β2-microglobulin closely correlated with urinary β2-microglobulin to creatinine ratio (Spearman's r= 0.91, 95% CI 0.84-0.95, P<0.001). The pH of urine samples was >5.5, a level at which degradation of urinary β2-microglobulin does not occur[44].

Acute kidney injury was defined according to KDIGO, as an increase in serum creatinine of ≥0.3 mg/dl (26.5 μmol/l) during hospitalization[45]. Hypophosphatemia was defined as serum phosphate level <0.81 mmol/l and hypouricemia as a serum uric acid level below 2.5 mg/dl. Inappropriate uricosuria and phosphaturia were defined as FE_{UA} >10% in patients with hypouricemia, or FE_{PO4} >20% in those with hypophosphatemia[24].

SARS-CoV-2 polymerase chain reaction

SARS-CoV-2 RNA detection in nasopharyngeal swabs was performed using COVID-19 genesig® Real-Time RT-PCR assay (Primerdesign Ltd, Chandler's Ford, United Kingdom) in a LightCycler 480 instrument (Roche Diagnostics, Mannheim, Germany). Primers and probe of this assay target the RNA-dependent RNA polymerase (RdRp) gene. A test with a cycle threshold less than 40 was considered positive.

Urine amino acids

Aminoaciduria was analyzed only in a subset of patients because (i) it requires non-automated, manual preparation of samples, with a potential risk of contamination for lab technicians; (ii) the method is labor intensive and time consuming, requiring ~270 min for each run, followed by additional time for data extraction. Urine amino acids were quantified by ion exchange chromatography with post column derivatization with Ninhydrin using a Biochrom 30 amino acid analyzer (Cambridge, England) in the routine workflow of the

Biochemical Genetics laboratory (Cliniques universitaires Saint-Luc UCLouvain). Amino acid excretion was normalized to creatinine (in mmol/mol creat).

Antibodies and reagents

The following antibodies were used: rabbit anti-human Gc-globulin (also known as VDBP, A0021, Dako); mouse anti-human ACE2 (AMAB91262, Sigma); rabbit anti-human ACE2 (AF933, R&D); rabbit anti-human AQP1 (ab2219, Millipore); sheep anti-LRP2 (gift from P. Verroust and R. Kozyraki, INSERM, Paris, France); rabbit anti-human UP1 (A0257, Dako); rabbit anti-human LMW proteins (A0126, Dako).

Immunoblot

Sodium dodecylsulfate-polyacrylamide gel electrophoresis and immunoblot were performed as previously described[46]. Urine samples were thawed on ice, diluted in Laemmli buffer and proteins separated by sodium dodecylsulfate-polyacrylamide gel electrophoresis (7.5%, 12% or 16% acrylamide slabs) in non-reducing conditions. The volume of urine loaded in each lane was normalized for creatinine concentration. After blotting onto nitrocellulose and blocking, membranes were incubated overnight at 4°C with primary antibody, washed, incubated with peroxidase-labeled secondary antibody, and visualized with enhanced chemiluminescence (ECL, Pierce, Aalst, Belgium).

Pathologic evaluation

Pathologic evaluation was performed on kidney samples obtained from autopsies of 6 COVID-19 cases. All specimens were well preserved without autolysis, and post-mortem interval was less than 6 hours. None of the patients received antiviral or nephrotoxic drug. Sections of formaldehyde-fixed paraffin-embedded blocks were stained with hematoxylin and

eosin, periodic acid-Schiff, Masson trichrome and Perls staining in all cases. Stained sections were evaluated for the number of total and sclerotic glomeruli; extent of interstitial fibrosis and tubular atrophy; presence of tubular lesions; alterations of the brush border; intra-luminal debris; vacuolization of tubular cells, erythrocytes aggregates; glomerular lesions; and interstitial inflammation[16]. All kidney sections were evaluated by an experienced kidney pathologist.

Electron microscopy

For electron microscopy, kidney samples obtained at autopsy from 2 patients deceased from COVID-19 were fixed in 2.5% glutaraldehyde in 0.1 M cacodylate buffer (pH 7.3) overnight. After rinsing in 0.1 M cacodylate buffer, kidney samples were post-fixed in 1% osmium tetroxide in cacodylate buffer for 40 min at room temperature, washed, and then stained with aqueous uranyl acetate for 1 hour at room temperature. After dehydration through a graded series of ethanol, samples were infiltrated and embedded in Epon812 (Sigma, Buchs, Switzerland) at 60°C for 28 hours. 350-nm semi-thin sections were cut with a Leica EM FCS ultra-microtome (Leica Microsystem, Germany) and stained with toluidine blue, followed by image acquisition by a Slidescanner (Zeiss Axio Scan.Z1, Germany) using 40x Plan Apochromat objective and image processing with ImageJ. 60-nm ultra-thin sections were collected onto formvar-coated copper grids, stained with lead phosphate dilution in water, and analyzed in an electron microscope (Philips CM100, Philips Electron Optics, Eindhoven, The Netherlands) at 80kV. The sample processing and image acquisition for toluidine blue staining and transmission electron microscopy were performed at the Center for Microscopy and Image Analysis of the University of Zurich (Zurich, Switzerland).

Immunostaining

Immunostaining was performed on formaldehyde-fixed paraffin-embedded sections of normal human kidney and kidney from patients with active COVID-19 using a sequential staining protocol as described previously[46]. Paraffin blocks were sectioned into consecutive 5-µm-thick slices on Superfrost Plus glass slides (Thermo Fisher Scientific). Before staining, slides were deparaffinized in decreasing concentrations of ethanol and antigen retrieval was performed by incubating in sodium citrate buffer (1.8% 0.1M citric acid, 8.2% 0.1M sodium citrate, in distillated water, pH 6.0) in a water bath for 30 min. The sections were blocked with phosphate-buffered saline (PBS) containing 5% BSA, and incubated for 1 hour with primary antibodies. After 3 PBS rinses, fluorophore-conjugated Alexa secondary antibodies (Invitrogen) were applied for 30 minutes. Negative controls were performed by omitting the primary antibody. Sections were subsequently mounted in ProLong Gold DAPI Antifade reagent (Invitrogen) and analyzed on a Zeiss LSM800 confocal microscope (Carl Zeiss), using x20/0.8 Plan-Apochromat (Carl Zeiss). Quantitative image analysis was performed using Zen 2 (blue edition) software (Carl Zeiss) by randomly selecting 5 visual fields per each slide that included at least three to five PTs, using constant setting parameters (i.e., pinhole, laser power, and offset gain and detector amplification below pixel saturation). URAT1 and B^0AT1 staining were obtained from the Human Protein Atlas[47], v15.proteinatlas.org, accessed on May 26, 2020.

Microdissection of mouse renal tubules, quantitative RT-PCR and interactome

The segmental expression of specific markers in mouse kidney was performed as described[48]. Kidneys of C57BL6J mice were digested with type-2 collagenase and tubules were isolated manually according to the morphological differences, before lysis in RNA extraction buffer from RNAqueous® Total RNA Isolation Kit (Invitrogen, Carlsbad, CA). Quantitative reverse transcription polymerase chain reaction was performed on pools of ~70 isolated renal tubules.

Total RNA was extracted from segments with RNAqueous^{R} kit (Applied Biosystems, Life Technologies). One µg of RNA was used to perform the reverse transcriptase reaction with iScript$^{\mathbf{TM}}$ cDNA Synthesis Kit (Bio-Rad). Changes in mRNA levels of the target genes were determined by relative RT-qPCR with a CFX96^{TM} Real-Time PCR Detection System (Bio-Rad) using iQ$^{\mathbf{TM}}$ SYBR Green Supermix (Bio-Rad). The analyses were performed in duplicate with 100nM of both sense and anti-sense primers in a final volume of 20µL using iQ^{TM} SYBR Green Supermix (Bio-Rad). Specific primers were designed using Primer3 (Suppl. Table 11). PCR conditions were 95°C for 3 min followed by 40 cycles of 15 sec at 95°C, 30 sec at 60°C. The PCR products were sequenced with the BigDye terminator kit (Perkin Elmer Applied Biosystems, Schwerzenbach, Switzerland) using ABI3100 capillary sequencer (Perkin Elmer Applied Biosystems). The efficiency of each set of primers was determined by dilution curves (Suppl. Table 11). The relative changes in targeted genes over *Gapdh* mRNAs were calculated using the $2^{-\Delta\Delta Ct}$ formula.

The connectivity network of the interactions between human SLC6A19 (B^0AT1) and other proteins including the SARS-Cov-2 receptor ACE2 and the related protein TMEM27 (collectrin), was established using the STRING (Search Tool for the Retrieval of Interacting Genes/Proteins) database[49].

Statistical analysis

Results are presented as means ± SD or median (IQR) for continuous variables and as numbers and proportions for categorical variables. Continuous variables were expressed in their natural units without standardization. Comparisons between groups were performed using unpaired t-test, Kruskal-Wallis, or $\chi 2$ test, as appropriate. Spearman's rank test was performed to assess the correlation between serum uric acid level and urinary fractional excretion of uric acid.

Time to event analyses were performed using Cox proportional hazard regressions (where events were defined as the need for invasive mechanical ventilation or death) and a competing risk approach. In the latter, the hazard ratio for invasive mechanical ventilation and its 95% confidence interval was estimated by including each specific PT defect and baseline characteristics as covariates and by considering death and discharge as competing events. Multivariable time to event analyses have been adapted to adjust for pre-specified relevant covariates including age, gender, baseline lymphocyte count, LDH and hsCRP levels. Collinearity between variables was quantified using variance inflation factors, and variance inflation factors >10 suggested excessive correlation between variables.

All statistical analyses were performed using GraphPad Prism (version 8.0) or Stata (version 16.0) software. All tests were two-tailed and a P-value <0.05 was considered significant.

DISCLOSURE

The authors declare no potential conflict of interest relevant to this article.

LIST OF PARTICIPANTS

CUSL COVID-19 Research Group: Frank Aboubakar, Souad Acid, Nadia Amini, Sarah Bailly, Christophe Beauloye, Diego Castanares-Zapatero, Emmanuel Coche, Christine Collienne, Pascale Cornette, Isabelle De Brauwer, Mélanie Dechamps, Florence Dupriez, Antoine Froidure, Quentin Garnir, Bernhard Gerber, Benoît Ghaye, Isabelle Gilard, Sophie Gohy, Charles Grégoire, Philippe Hantson, Luc-Marie Jacquet, Benoit Kabamba, Shakeel Kautbally, Nicolas Lanthier, Fatima Larbaoui, Giuseppe Liistro, Frédéric Maes, Virginie Montiel, Benny Mwenge, Sophie Pierard, Charles Pilette, Anne Catherine Pouleur, Amaury Sogorb, Peter Starkel, Hector Rodriguez-Villalobos, Maximilien Thoma, Olivier Van Caeneghem, David Vancraeynest.

ACKNOWLEDGEMENTS

We wish to thank Yvette Cnops, Huguette Debaix and Sebastien Druart for expert technical assistance; Cynthia S. Goldsmith (Centers for Disease Control and Prevention, Atlanta, GA, USA), Andres Kaech (University of Zurich, Zurich), Johannes Loffing (University of Zurich, Zurich), John Shelburne (Durham Veterans Administration Hospital, Durham, NC, USA), Marie-Francoise Vincent (UCLouvain, Brussels), for helpful discussions; and Caroline Bouzin and Arthur Colson, for image acquisition and analysis. Imaging was performed at the IREC Imaging platform at UCLouvain (Brussels, Belgium), and with equipment maintained by the Center for Microscopy and Image Analysis, University of Zurich (Zurich, Switzerland).

AUTHORS' CONTRIBUTIONS

Designed the study: AW, OD, MJ and JM; took care of the patients: AW, LB, MP, AP, JDG, HY, LP, JCY, LG, XW, PFL, and JM; collected clinical data: AW, MP, JM; performed post-mortem examinations: GS and SA; assessed and interpreted urine amino acids: JD, OD and JM; performed and interpreted SARS-CoV-2 PCR: AS; performed, supervised and analyzed experiments: ZC, SEM, OD and JM; performed statistical analyses: JM. Each author contributed important intellectual content during manuscript drafting or revision and agrees to be personally accountable for the individual's own contributions and to ensure that questions pertaining to the accuracy or integrity of any portion of the work, even one in which the author was not directly involved, are appropriately investigated and resolved, including with documentation in the literature if appropriate.

FUNDING

JM is supported by the Fonds National pour la Recherche Scientifique (JM), the Fondation Saint-Luc (JM), the Fonds de Recherche Clinique des Cliniques universitaires Saint-Luc (JM), and the Association pour l'Information et la Recherche sur les maladies rénales Génétiques (JM). OD is supported by the European Reference Network for Rare Kidney Diseases (ERKNet) – project ID N° 739532; the Cystinosis Research Foundation (USA); the NCCR Kidney.CH program (Swiss National Science Foundation); and the Swiss National Science Foundation 310030-189044. The funders had no role in study design, data collection, analysis, reporting, or the decision to submit for publication.

Supplementary Material

Supplementary Figures S1-S5
Supplementary Tables S1-S11
Supplementary information is available at *Kidney International*'s website.

REFERENCES

1. Acter T, Uddin N, Das J, et al. Evolution of severe acute respiratory syndrome coronavirus 2 (SARS-CoV-2) as coronavirus disease 2019 (COVID-19) pandemic: A global health emergency. Sci Total Environ. 2020;730:138996. doi: 10.1016/j.scitotenv.2020.138996.
2. Wu Z, McGoogan JM. Characteristics of and Important Lessons From the Coronavirus Disease 2019 (COVID-19) Outbreak in China: Summary of a Report of 72 314 Cases From the Chinese Center for Disease Control and Prevention. JAMA. 2020, in press. doi: 10.1001/jama.2020.2648.
3. Guan WJ, Ni ZY, Hu Y, et al. Clinical Characteristics of Coronavirus Disease 2019 in China. N Engl J Med. 2020;382:1708-1720. doi:10.1056/NEJMoa2002032.
4. Li W, Moore MJ, Vasilieva N, Sui J, et al. Angiotensin-converting enzyme 2 is a functional receptor for the SARS coronavirus. Nature. 2003 Nov 27;426(6965):450-4. doi:10.1038/nature02145.
5. Hamming I, Timens W, Bulthuis ML, et al. Tissue distribution of ACE2 protein, the functional receptor for SARS coronavirus. A first step in understanding SARS pathogenesis. J Pathol. 2004;203:631-637. doi:10.1002/path.1570.
6. Yan R, Zhang Y, Li Y, et al. Structural basis for the recognition of SARS-CoV-2 by full-length human ACE2. Science. 2020;367:1444-1448. doi: 10.1126/science.abb2762.
7. Lan J, Ge J, Yu J, et al. Structure of the SARS-CoV-2 spike receptor-binding domain bound to the ACE2 receptor. Nature. 2020, in press. doi: 10.1038/s41586-020-2180-5.
8. Diao B, Wang C, Wang R, et al. Human Kidney is a Target for Novel Severe Acute Respiratory Syndrome Coronavirus 2 (SARS-CoV-2) Infection. medRxiv 2020.03.04.20031120; doi: 10.1101/2020.03.04.20031120.
9. Naicker S, Yang CW, Hwang SJ, et al. The Novel Coronavirus 2019 epidemic and kidneys. Kidney Int. 2020;97:824-828. doi: 10.1016/j.kint.2020.03.001.
10. Cheng Y, Luo R, Wang K, et al. Kidney disease is associated with in-hospital death of patients with COVID-19. Kidney Int. 2020;97:829-838. doi: 10.1016/j.kint.2020.03.005.
11. Pei G, Zhang Z, Peng J, et al. Renal Involvement and Early Prognosis in Patients with COVID-19 Pneumonia. J Am Soc Nephrol. 2020, in press. doi: 10.1681/ASN.2020030276.
12. Li Z, Wu M, Yao J, Get al. Caution on Kidney Dysfunctions of COVID-19 Patients medRxiv 2020.02.08.20021212; doi: https://doi.org/10.1101/2020.02.08.20021212
13. Gross O, Moerer O, Weber M, et al. COVID-19-associated nephritis: early warning for disease severity and complications? Lancet. 2020;395:e87-e88. doi:10.1016/S0140-6736(20)31041-2.
14. Tay MZ, Poh CM, Rénia L, et al. The trinity of COVID-19: immunity, inflammation and intervention. Nat Rev Immunol. 2020;20:363-374. doi:10.1038/s41577-020-0311-8.
15. Puelles VG, Lütgehetmann M, Lindenmeyer MT, et al. Multiorgan and Renal Tropism of SARS-CoV-2. N Engl J Med. 2020, in press. doi:10.1056/NEJMc2011400

16. Su H, Yang M, Wan C, et al. Renal histopathological analysis of 26 postmortem findings of patients with COVID-19 in China. Kidney Int. 2020, in press. doi: 10.1016/j.kint.2020.04.003.
17. Farkash EA, Wilson AM, Jentzen JM. Ultrastructural Evidence for Direct Renal Infection with SARS-CoV-2. J Am Soc Nephrol. 2020, in press. doi: 10.1681/ASN.2020040432.
18. Smith KD, Shreeram Akilesh S, Charles E. Alpers CE, et al. Am I a Coronavirus? Kidney Int 2020, in press. doi:10.1016/j.kint.2020.05.021.
19. Miller SE, Brealey JK. Visualization of putative coronavirus in kidney. Kidney Int 2020, in press. doi:10.1016/j.kint.2020.05.004.
20. Goldsmith CS, Miller SE, Martines RB, et al. Electron microscopy of SARS-CoV-2: a challenging task. Lancet. 2020;395:e99. doi:10.1016/S0140-6736(20)31188-0.
21. Revel MP, Parkar AP, Prosch H, et al. COVID-19 patients and the radiology department - advice from the European Society of Radiology (ESR) and the European Society of Thoracic Imaging (ESTI). Eur Radiol. 2020, in press. doi: 10.1007/s00330-020-06865-y.
22. Kleta R, Romeo E, Ristic Z, et al. Mutations in SLC6A19, encoding B0AT1, cause Hartnup disorder. Nat Genet. 2004;36:999-1002. doi: 10.1038/ng1405.
23. Singer D, Camargo SM. Collectrin and ACE2 in renal and intestinal amino acid transport. Channels (Austin). 2011;5:410-23. doi: 10.4161/chan.5.5.16470.
24. van der Wijst J, Belge H, Bindels RJM, Devuyst O. Learning Physiology From Inherited Kidney Disorders. Physiol Rev. 2019;99:1575-1653. doi: 10.1152/physrev.00008.2018.
25. Nielsen R, Christensen EI, Birn H. Megalin and cubilin in proximal tubule protein reabsorption: from experimental models to human disease. Kidney Int. 2016;89:58-67. doi: 10.1016/j.kint.2015.11.007.
26. Forster IC, Hernando N, Biber J, Murer H. Phosphate transporters of the SLC20 and SLC34 families. Mol Aspects Med. 2013 Apr-Jun;34(2-3):386-95. doi: 10.1016/j.mam.2012.07.007.
27. De Matteis MA, Staiano L, Emma F, Devuyst O. The 5-phosphatase OCRL in Lowe syndrome and Dent disease 2. Nat Rev Nephrol. 2017 Aug;13(8):455-470. doi: 10.1038/nrneph.2017.83.
28. Festa BP, Chen Z, Berquez M, et al. Impaired autophagy bridges lysosomal storage disease and epithelial dysfunction in the kidney. Nat Commun. 2018 Jan 11;9(1):161. doi: 10.1038/s41467-017-02536-7.
29. Festa BP, Berquez M, Gassama A, et al. OCRL deficiency impairs endolysosomal function in a humanized mouse model for Lowe syndrome and Dent disease. Hum Mol Genet. 2019;28:1931-1946. doi:10.1093/hmg/ddy449.
30. Chen Z, Luciani A, Mateos JM, et al. Transgenic zebrafish modeling low-molecular-weight proteinuria and lysosomal storage diseases. Kidney Int. 2020;97:1150-1163. doi:10.1016/j.kint.2019.11.016
31. Cez A, Brocheriou I, Lescure FX, et al. Decreased expression of megalin and cubilin and altered mitochondrial activity in tenofovir nephrotoxicity. Hum Pathol. 2018;73:89-101. doi:10.1016/j.humpath.2017.12.018.

32. Hoffmann M, Kleine-Weber H, Schroeder S, et al. SARS-CoV-2 Cell Entry Depends on ACE2 and TMPRSS2 and Is Blocked by a Clinically Proven Protease Inhibitor. Cell. 2020;181:271-280.e8. doi:10.1016/j.cell.2020.02.052.
33. Karimian Pour N, McColl ER, Piquette-Miller M. Impact of Viral Inflammation on the Expression of Renal Drug Transporters in Pregnant Rats. Pharmaceutics. 2019;11:E624. doi: 10.3390/pharmaceutics11120624.
34. Ling Y, Xu SB, Lin YX et al. Persistance and clearance of viral RNA in 2019 novel coronavirus disease rehabilitation patients. Chin Med J (Engl). 2020 May 5;133(9):1039-1043. doi: 10.1097/CM9.0000000000000774.
35. Sun J, Zhu A, Li H, et al. Isolation of infectious SARS-CoV-2 from urine of a COVID-19 patient. Emerg Microbes Infect. 2020 Apr 28:1-8. doi: 10.1080/22221751.2020.1760144.
36. Monteil V, Kwon H, Prado P, et al. Inhibition of SARS-CoV-2 Infections in Engineered Human Tissues Using Clinical-Grade Soluble Human ACE2. Cell. 2020 Apr 17. pii: S0092-8674(20)30399-8. doi: 10.1016/j.cell.2020.04.004.
37. Kissling S, Rotman S, Gerber C, et al. Collapsing glomerulopathy in a COVID-19 patient. Kidney Int 2020, in press. doi:10.1016/j.kint.2020.04.006.
38. Oshiro LS, Schieble JH, Lennette EH. Electron microscopic studies of coronavirus. J Gen Virol. 1971;12:161-168. doi:10.1099/0022-1317-12-2-161.
39. Goldsmith CS, Tatti KM, Ksiazek TG, et al. Ultrastructural characterization of SARS coronavirus. Emerg Infect Dis. 2004;10:320-326. doi:10.3201/eid1002.030913.
40. Haguenau, F. "Virus-like" particles as observed with the electron microscope. in: A.J. Dalton, F. Haguenau (Eds.) Ultrastructure of Animal Viruses and Bacteriophages. Academic Press, Waltham, MA; 1973: 391–397.
41. Miller SE. Problems and pitfalls in diagnostic electron microscopy. Microsc Microanal. 2012; 18:172–173.
42. Wu VC, Huang JW, Hsueh PR, et al. Renal hypouricemia is an ominous sign in patients with severe acute respiratory syndrome. Am J Kidney Dis. 2005;45:88-95. 10.1053/j.ajkd.2004.09.031.
43. Igarashi T. Fanconi syndrome. In: Pediatric Nephrology. Avner ED, Harmon WE, Niaudet P, Yoshikawa N (Eds.), Springer-Verlag, Berlin Heidelberg, 2009, pp. 1039-1067.
44. Portman RJ, Kissane JM, Robson AM. Use of beta 2 microglobulin to diagnose tubulo-interstitial renal lesions in children. Kidney Int. 1986;30:91-98. doi:10.1038/ki.1986.156.
45. Ostermann M, Bellomo R, Burdmann EA, et al. Controversies in Acute Kidney Injury: Conclusions from a Kidney Disease Improving Global Outcomes (KDIGO) Conference. Kidney Int 2020; in press. doi: 10.1016/j.kint.2020.04.020.
46. Morelle J, Sow A, Hautem N, et al. Interstitial Fibrosis Restricts Osmotic Water Transport in Encapsulating Peritoneal Sclerosis. J Am Soc Nephrol. 2015;26:2521-33. doi: 10.1681/ASN.2014090939.
47. Uhlén M, Fagerberg L, Hallström BM, et al. Proteomics. Tissue-based map of the human proteome. Science. 2015;347:1260419. doi:10.1126/science.1260419
48. Tokonami N, Takata T, Beyeler J, et al. Uromodulin is expressed in the distal convoluted tubule, where it is critical for regulation of the sodium chloride cotransporter NCC. Kidney Int. 2018;94:701-715. doi: 10.1016/j.kint.2018.04.021.

49. Szklarczyk D, Gable AL, Lyon D, et al. STRING v11: protein-protein association networks with increased coverage, supporting functional discovery in genome-wide experimental datasets. Nucleic Acids Res. 2019;47:D607□D613. doi:10.1093/nar/gky1131.

FIGURE LEGENDS

Figure 1. Proximal tubule dysfunction in patients with COVID-19.

A. Prevalence (%) of signs of proximal tubule (PT) dysfunction in patients with active COVID-19. Uβ2M, urinary β2-microglobulin; UPCR, urinary protein to creatinine ratio; UAPR, urinary albumin to protein ratio; HypoU, hypouricemia; inappr. UAuria, inappropriate uricosuria; HypoP, hypophosphatemia; inappr. Puria; inappropriate phosphaturia; AAuria; aminoaciduria. Numbers (n) of patients tested are shown in brackets inside the bars.

B. Distribution of urinary ß2-microglobulin ($U\beta_2M$), urinary protein to creatinine ratio (UPCR) and urinary albumin to protein ratio (UAPR), and relationship between $U\beta_2M$ and urinary albumin to creatinine ratio in patients with COVID-19. Circles represent individual values and red lines medians.

C. Inverse relationship between the lowest serum uric acid (sUA) level and fractional excretion of uric acid (FE_{UA}) in patients with (grey circles) and without (open circles) hypouricemia. Spearman's coefficient, r = -0.79 (95% CI -0.89, -0.63), P<0.001, n=39.

D. Sodium dodecyl sulfate polyacrylamide gel electrophoresis followed by Coomassie blue staining and immunoblot shows the presence of low-molecular weight proteins (LMWP), vitamin D binding protein (VDBP), and Clara cell secretory protein (CC16). Normal urine and urine from a patient with Dent disease (a rare inherited PT dysfunction caused by *CLCN5* mutation) are shown as controls. Molecular weights (in kDa) of the urinary proteins are provided.

E. Relative urinary concentration of amino acids in patients with COVID-19 and aminoaciduria (COVID-19^+/uAA^+, back bars) or no aminoaciduria (COVID-19^+/uAA^-, open bars). The reference corresponds to the upper limit of normal. Individual values are represented by circles and bars represent the mean values.

Figure 2. Proximal tubule damage in kidneys of COVID-19 patients.

A. Pathologic scoring of kidney lesions in COVID-19. The grid summarizes pathologic findings on post-mortem examination in 6 patients with COVID-19 and the presence (grey) or absence (white) of tubular injury, brush border loss, debris in the lumen, red blood cells (RBC) aggregates, vacuolization of tubular cells, and glomerular (glom.) alterations. Representative pictures of sections from control and COVID-19 kidneys, stained with Periodic Acid Schiff (PAS) or Masson's trichrome staining (MTS), show prominent tubular lesions with dilation, mitoses in epithelial cells, major alterations of the brush border (i.e. in

the S1 segment of the PT), shedding of cellular debris into the lumen, as well as erythrocytes aggregates in peritubular capillaries. M, male; F, female. Original magnification, 20x and 40x; scale bars, 50 µm and 25 µm, on left and right pictures, respectively.

B. Representative pictures of double immunostaining with anti-AQP1 (green channel) and anti-megalin (LRP2, red channel) antibodies viewed under confocal fluorescence microscopy in kidney sections from a control and a patient with COVID-19. Nuclei are stained with DAPI (blue channel). Original magnification, 20x. Bars, 50 µm. Mean fluorescence intensity (M.F.I.) profiles and relative maximal intensity (rel. max. int.) for LRP2 were quantified on cross-sectional sections of PT from 3 controls (grey) and 5 patients who died of COVID-19 (red). Data are mean values and s.e.m. P=0.002, unpaired t-test.

Figure 3. Transmission electron microscopy of particles in proximal tubule cells in a kidney sample of an autopsied patient deceased from COVID-19.

A. Low magnification electron microscopy image showing numerous particles of approximately 90-140 nm in diameter within the lumen of rough endoplasmic reticulum (RER) (arrows), some of which have budded into the lumen from the cytoplasm (arrowheads). Inset (a) shows the budding and the stalk of a particle. Size is indicated by the magnification bars.

B. Particles observed inside vacuoles formed by RER and lighter densities inside smooth ER. Areas seen in the lower magnification marked by dash-lined boxes are enlarged in solid-lined insets and are labeled correspondingly. Insets a and b are representative of numerous particles containing dense smudgy dots in similarly sized particles observed within RER elsewhere. In some particles (a), the trilaminar membrane envelope is evident. A larger vacuole (c) without ribosomes studding the outside and located near the Golgi apparatus contains irregularly sized densities and does not contain viruses. Size of the low magnification is indicated on the print; size in the high magnifications is the same in all insets and is indicated by the bar in a.

C. Particles shown (similarly as in B above), at low magnification in the large image in dashed-lined boxes and at high magnification in solid-lined insets corresponding to the dashed boxes. All particles have irregular dense black dots inside, and a few (e.g., see b, e) have crisp small rings, possibly exact cross sections of tubular or helical structures. Size of the low magnification is indicated on the print; size in the high magnifications is the same in all insets and is indicated by the bar in f.

Table 1. Baseline characteristics of the 49 patients with specific urinalysis.

Demographics and comorbidities	**n=49**
Age, median (IQR), years	64 (54-74)
Male gender – no. (%)	34 (69)
Ethnicity – no. (%)	
Caucasian	42 (86)
Sub-Saharan African	6 (12)
Other	1 (2)
Cardiovascular disease – no. (%)	9 (18)
Chronic kidney disease – no. (%)	7 (14)
Hypertension – no. (%)	23 (47)
Diabetes – no. (%)	10 (20)
Human immunodeficiency virus infection – no. (%)	0 (0)
Chronic liver disease – no. (%)	1 (2)
Chronic pulmonary disease – no. (%)	5 (12)
Medications – no. (%)	
Allopurinol or febuxostat	4 (8)
Angiotensin receptor blocker	10 (20)
ACE inhibitor	10 (20)
Chronic immunosuppressive treatment[a]	4 (8)
Anti-cancer drugs[b]	4 (8)
Symptoms and vitals at admission	
Duration of symptoms, median (IQR), days	7 (3-9)
Symptoms at admission – no. (%)	
Fever	39 (80)
Cough	29 (59)
Dyspnea	35 (71)
Sore throat	2 (4)
Confusion	6 (12)
Anosmia/agueusia	6 (12)
Rhinitis	7 (14)
Diarrhea	14 (29)

Chest pain	4 (8)
Admission via emergency department – no. (%)	47 (96)
Sa02, median (IQR), %	92 (87-96)
Systolic BP, median (IQR), mmHg	139 (126-150)
Diastolic BP, median (IQR), mmHg	75 (69-82)
Heart rate, median (IQR), bpm	93 (88-103)
Lab tests and dipstick urinalysis at admission	
hsCRP, median (IQR), mg/l	105 (54-146)
Glycemia, median (IQR), mg/dl	121 (109-146)
Serum creatinine, median (IQR), mg/dl	1.0 (0.8-1.2)
eGFR, median (IQR), ml/min/1.73 m2	72 (54-92)
Serum uric acid, median (IQR), mg/dl	4.9 (3.3-5.9)
Sodium, median (IQR), mmol/l	135 (133-138)
Bicarbonate, median (IQR), mmol/l	23 (22-25)
AST, median (IQR), IU/l	36 (24-53)
ALT, median (IQR), IU/l	27 (17-46)
Total bilirubin, median (IQR), mg/dl	0.5 (0.4-0.7)
CK, median (IQR), IU/l	119 (74-211)
LDH, median (IQR), IU/l	356 (279-491)
Lymphocytes, median (IQR), n/µl	650 (500-1060)
Platelets, median (IQR), 10^3/µl	203 (131-233)
Dipstick proteinuria – no. (%)	
0	8/43 (19)
1+	13/43 (30)
2+	19/43 (44)
3+	3/43 (7)
Computed tomography scan of the chest upon admission	
Extent of lesions on chest CT scan – no. (%)	
<10%	4/45 (9)
10-25%	18/45 (40)
25-50%	14/45 (31)
>50%	9/45 (20)
Drugs received for COVID-19	

Hydroxychloroquine – no. (%)	48 (98)
Azithromycin – no. (%)	7 (14)
Anti-viral drugs – no. (%)	0 (0)
Immunomodulatory drugs[c] - no. (%)	16 (33)

[a]Chronic immunosuppressive treatment included (one or more per patient) ciclosporin A (1), corticosteroids (2), methotrexate (1), rituximab (1). [b]Anti-cancer drugs included cyclophosphamide (1), doxorubicine (1), vincristine (1), venetoclax (1), cisplatin (1), and cytarabine (1). [c]Immunomodulatory drugs for COVID-19 (one or more per patient) included corticosteroids (7), interleukin-7 (8), tocilizumab (1). Continuous variables are expressed as median and interquartile range (IQR), and categorical variables as numbers (no.) and percentages (%). Sa02, oxygen saturation while breathing ambient air; BP, blood pressure; eGFR, CKD-EPI estimated glomerular filtration rate; hsCRP, highly-sensitive C-reactive protein; AST, aspartate aminotransferase; ALT, alanine aminotransferase; CK, creatine kinase; LDH, lactate dehydrogenase; CT, computed tomography.

Table 2. Prevalence of proximal tubule dysfunction in COVID-19.

	n tested	n positive (%)
Urinary β2-microglobulin ($U\beta_2M$) >0.30 mg/l	49	33 (67)
Urinary protein to creatinine ratio (UPCR) >0.2 g/g	48	41 (85)
Urinary albumin to protein ratio (UAPR) <0.5	47	46 (98)
Hypouricemia	49	23 (47)
With inappropriate uricosuria	39	18 (46)
Hypophosphatemia	48	27 (56)
With inappropriate phosphaturia	32	6 (19)
Aminoaciduria	13	6 (46)
LMW proteinuria on SDS-PAGE	15	10 (67)
Normoglycemic glucosuria	43	0 (0)

LMW, low molecular weight; SDS-PAGE, sodium dodecyl sulfate polyacrylamide gel electrophoresis. Hypouricemia with inappropriate uricosuria, as serum uric acid <2.5 mg/dl and fractional excretion of uric acid >10%; and inappropriate phosphaturia as serum phosphate <0.81 mmol/l and a fractional excretion of phosphate >20%.

Fig. 1.

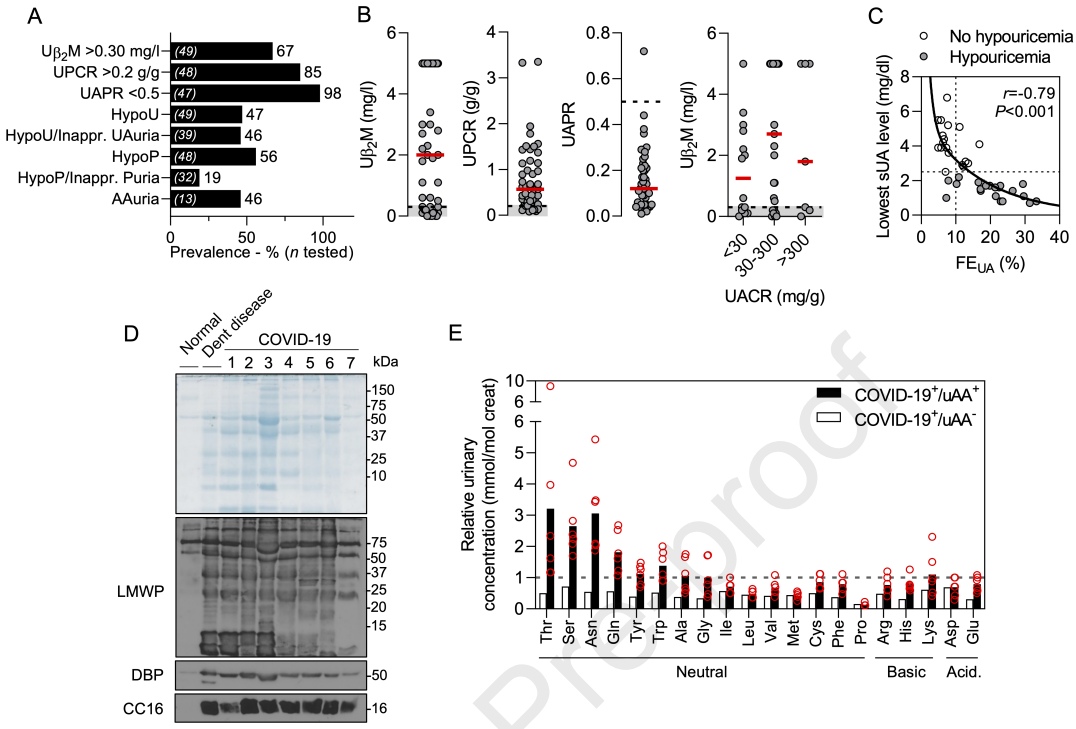

Fig. 2.

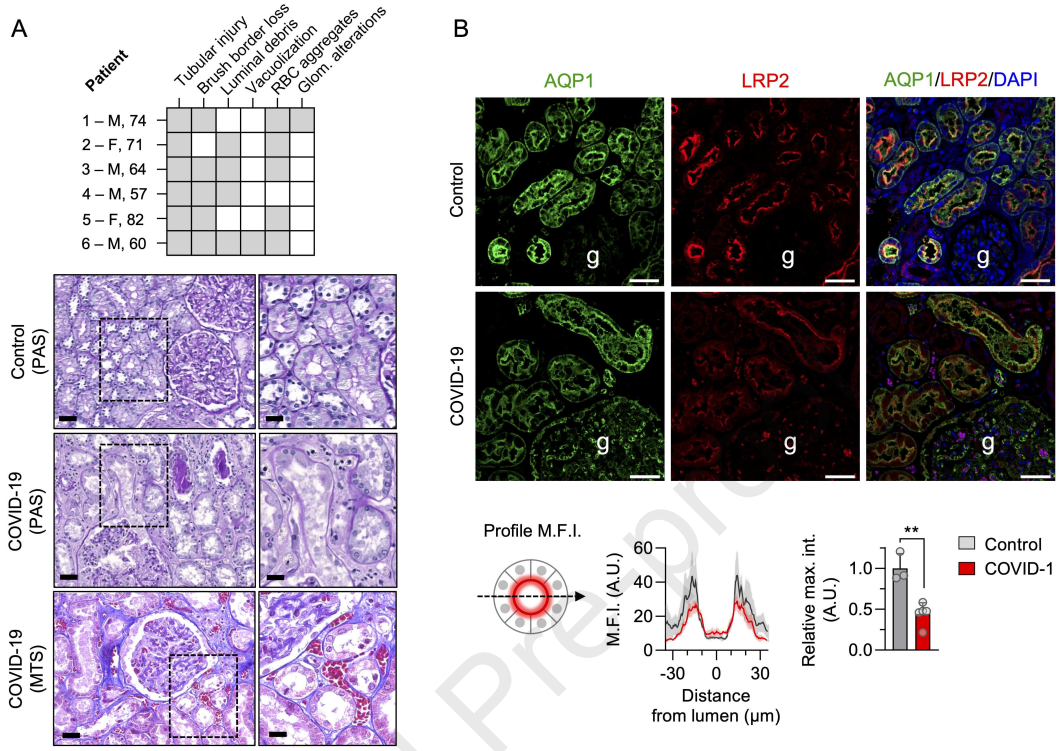

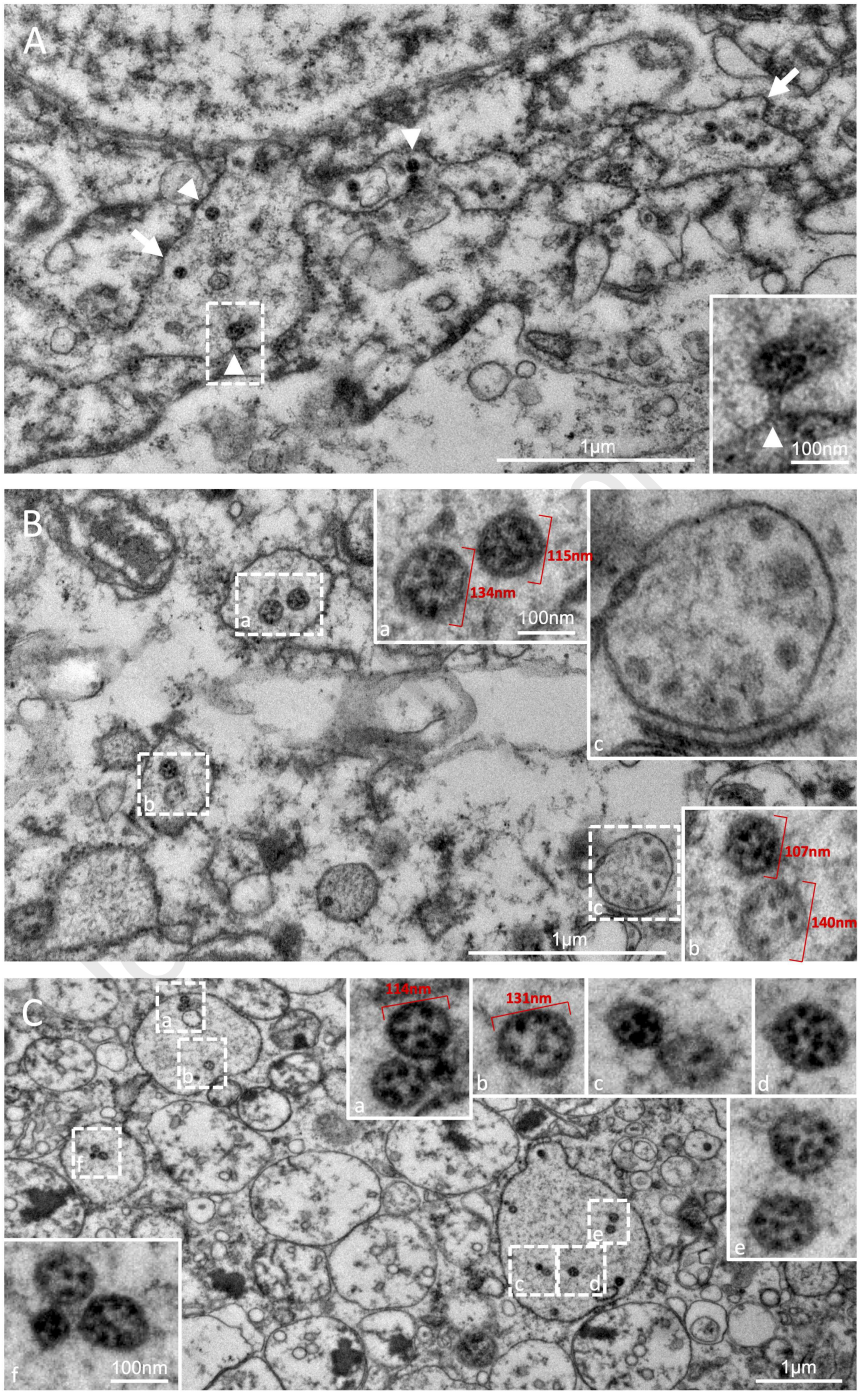
A
1μm
100nm
B
a
115nm
134nm
100nm
c
b
c
1μm
107nm
140nm
b
C
a
b
f
114nm
131nm
a
b
c
d
e
e
c
d
f
100nm
1μm